Materials and Design 32 (2011) 696–705

Contents lists available at ScienceDirect

Materials and Design

journal homepage: www.elsevier.com/locate/matdes

The microstructure evolution and nucleation mechanisms of dynamic recrystallization in hot-deformed Inconel 625 superalloy

Defu Li *, Qingmiao Guo, Shengli Guo, Haijian Peng, Zhigang Wu

General Research Institute for Non-ferrous Metals, Beijing 100088, PR China

ARTICLE INFO

Article history:
Received 31 May 2010
Accepted 31 July 2010
Available online 6 August 2010

Keywords:
A. Non-ferrous metals and alloys
B. Wrought
F. Microstructure

ABSTRACT

Hot compressions tests of Inconel 625 superalloy were conducted using a Gleeble-1500 simulator at different strains between 900 °C and 1200 °C with a strain rate of 0.1 s^{-1}. Optical microscope, transmission electron microscope and electron backscatter diffraction technique were employed to investigate the microstructure evolution and nucleation mechanisms of dynamic recrystallization. It was found that both the size and fraction of dynamically recrystallized grains increase with increasing deformation temperature. However, the size of dynamically recrystallized grains almost remains constant with increasing deformation strain. The dominant nucleation mechanism of dynamic recrystallization in Inconel 625 superalloy deformed at 1150 °C is the discontinuous dynamic recrystallization, which is characterized by the bulging of the original grain boundaries accompanied with twining. The continuous dynamic recrystallization characterized by progressive subgrain rotation occurs simultaneously in dynamic recrystallization process, although it can only be considered as an assistant nucleation mechanism at the early stage of hot deformation.

1. Introduction

Nickel-based superalloy Inconel 625 was developed as a solid-solution-strengthened alloy containing relatively high levels of chromium, molybdenum, carbon and niobium [1,2]. It is widely used in aeronautical, aerospace, chemical, petrochemical and marine applications, due to its good mechanical properties, processability, weldability and resistance to high temperature corrosion on prolonged exposure to aggressive environments [3,4]. To obtain a superior performance, the microstructure of the alloy during hot deformation should be controlled [5–8], which is closely related to the dynamic recrystallization (DRX) process [9–14]. Thus, much attention has been paid to the nucleation mechanism of DRX in nickel-based superalloy.

Recently, the microstructure characteristics, recrystallization behavior and mechanisms of DRX in nickel-based superalloys have been extensively studied by hot torsion or hot compression [15–18]. However, there are few reports on the microstructure evolution and the exact operating mechanisms of DRX in Inconel 625 superalloy during hot deformation. The aim of the present study is to investigate the influence of temperature and strain on the DRX microstructure evolution of Inconel 625 superalloy during hot deformation, and to clarify the nucleation mechanisms of DRX.

2. Experimental

2.1. Specimen and heat treatment

A forging bar of Inconel 625 superalloy with a nominal diameter of 200 mm is used in the present study, and the chemical compositions of the specimen are listed in Table 1. A mixture of extensively serrated and bulging grains is the main feature of the as-received materials, although some deformation twins are also observed, as shown in Fig. 1.

Cylindrical specimens with dimension of Φ 8 × 12 mm were machined from the center part of the forging bar. The specimens were annealed at 1200 °C for 30 min followed by water quenching to room temperature to obtain a fine homogeneous γ phase with carbides solute in the matrix. Equiaxed grains are presented in the annealed Inconel 625 superalloy with an average grain size of 81 μm, and some annealing twins also exist, as shown in Fig. 2.

2.2. Hot compression and microstructure characterization

Hot compression tests were carried out on a Gleeble-1500 simulator at different strains between 900 °C and 1200 °C with a strain rate of 0.1 s^{-1}. Based on the deformation map of nickel-based superalloy [8], the lowest deformation temperature is selected as 900 °C to induce the DRX process during deformation. Each specimen was heated to the setting temperatures at a rate of 10 °C/min by high frequency induction heating equipment attached to the

* Corresponding author. Tel.: +86 10 82241289; fax: +86 10 62012579.
E-mail address: lide_fu@163.com (D. Li).

0261-3069/$ - see front matter © 2010 Elsevier Ltd. All rights reserved.
doi:10.1016/j.matdes.2010.07.040

Table 1
The chemical compositions of Inconel 625 superalloy (wt.%).

C	Cr	Mo	Nb	Fe	Mg	Al	Mn	Si	Ti	Ni
0.053	21.32	8.58	3.73	0.11	0.01	0.18	0.04	0.09	0.16	Residual

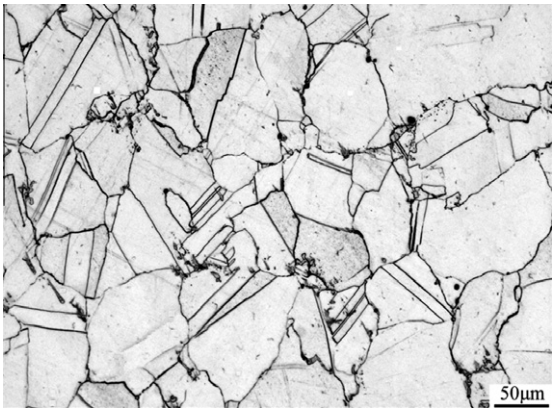

Fig. 1. Typical optical micrograph of the as-received Inconel 625 superalloy.

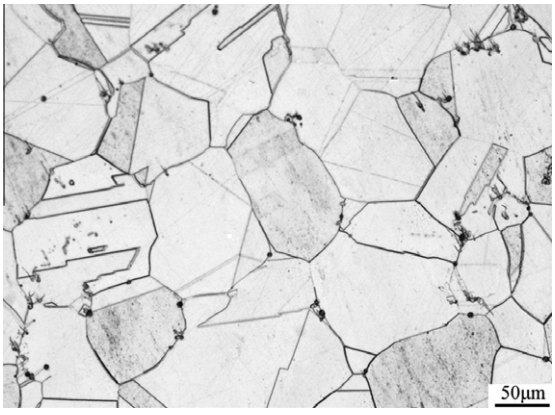

Fig. 2. Typical optical micrograph of the annealed Inconel 625 superalloy.

Gleeble-1500 simulator, and then held in the chamber for 3 min to ensure the temperature uniformity. During the hot compression, a thermocouple was welded on each specimen to record the real-time temperature. Meanwhile, the isothermal deformation process was achieved through closed-loop temperature control system of the Gleeble-1500 simulator. The load-stoke data were converted into true stress and true strain data through the controlling computer equipped with an automatic data acquisition system. After hot compression, the specimens were water quenched to room temperature to keep the hot-deformed microstructures. Then, the deformed specimens were sliced along the compression axis for microstructure characterization.

The sliced specimens were grinded, mechanically polished and then etched in a solution consisting of 10 ml H_2SO_4 + 100 ml HCl + 10 g $CuSO_4$ at room temperature for 5–10 s for metallographic observation, which were conducted using a LEICA-2100 optical microscope. The sliced specimens in the shape of 3 mm diameter discs for TEM observation were grinded and thinned using a twin-jet technique in the electrolyte of 10% $HClO_4$ and 90% ethanol solution at −15 °C with a current of 6–7 mA. TEM examination was conducted using TEM-2000 EX operated at 160 kV. EBSD measurements were carried out using a LEO-1450 electron probe equipped with Channel 5 software provided by HKL technology at the accelerating voltage of 30 kV. The orientation imaging microscopy (OIM) maps and misorientation angle of grains and subgrains can be calculated from the EBSD results. The specimen for EBSD investigation was electropolished in a 20% H_2SO_4 and 80% methanol solution at 20–30 V for 5–10 s at room temperature.

3. Results and discussion

3.1. Stress–strain behavior

The stress–strain curves of Inconel 625 superalloy compressed to a 0.7 true strain between 900 °C and 1200 °C at a strain rate of 0.1 s^{-1} are shown in Fig. 3. Typically, the flow stress increases to a maximum (peak stress) and then gradually decreases or even keeps constant at high strain zone. Such flow behavior for Inconel 625 superalloy belongs to those of normal behavior for alloys with low stacking fault energy, indicating the hot working is accompanied with DRX [19,20]. At lower deformation temperature (900 °C), the flow curve exhibits a high peak stress at a high peak strain. After the peak stress, the flow stress keeps constant with increasing strain, indicating that the work softening is insignificant. At higher deformation temperatures (950 °C, 1000 °C), work softening is more significant though the peak stress and peak strain are still high. When the deformation temperature increases to 1050–1200 °C, steady state is attained after small peak stress and peak strain with little work softening. The peak stress and the corresponding peak strain decrease with increasing the deformation temperature, which is consistent with those reported on the nickel-based superalloys [15–19].

3.2. The effect of temperature on dynamic recrystallization

Fig. 4 shows the optical microstructures of Inconel 625 superalloy deformed to a 0.7 true strain at different temperatures with a strain rate of 0.1 s^{-1}. First of all, the deformation microstructure depends closely on the deformation temperature, and the recrystallization starts from the grain boundaries. At 900 °C, bulging grain boundaries are the dominant feature as shown in Fig. 4a,

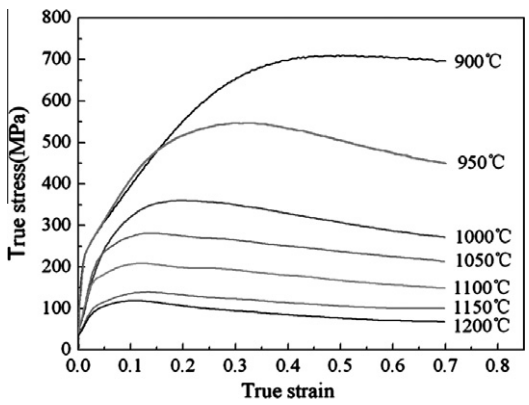

Fig. 3. The stress–strain curves of Inconel 625 superalloy deformed to a 0.7 true strain at different temperatures with a strain rate of 0.1 s^{-1}.

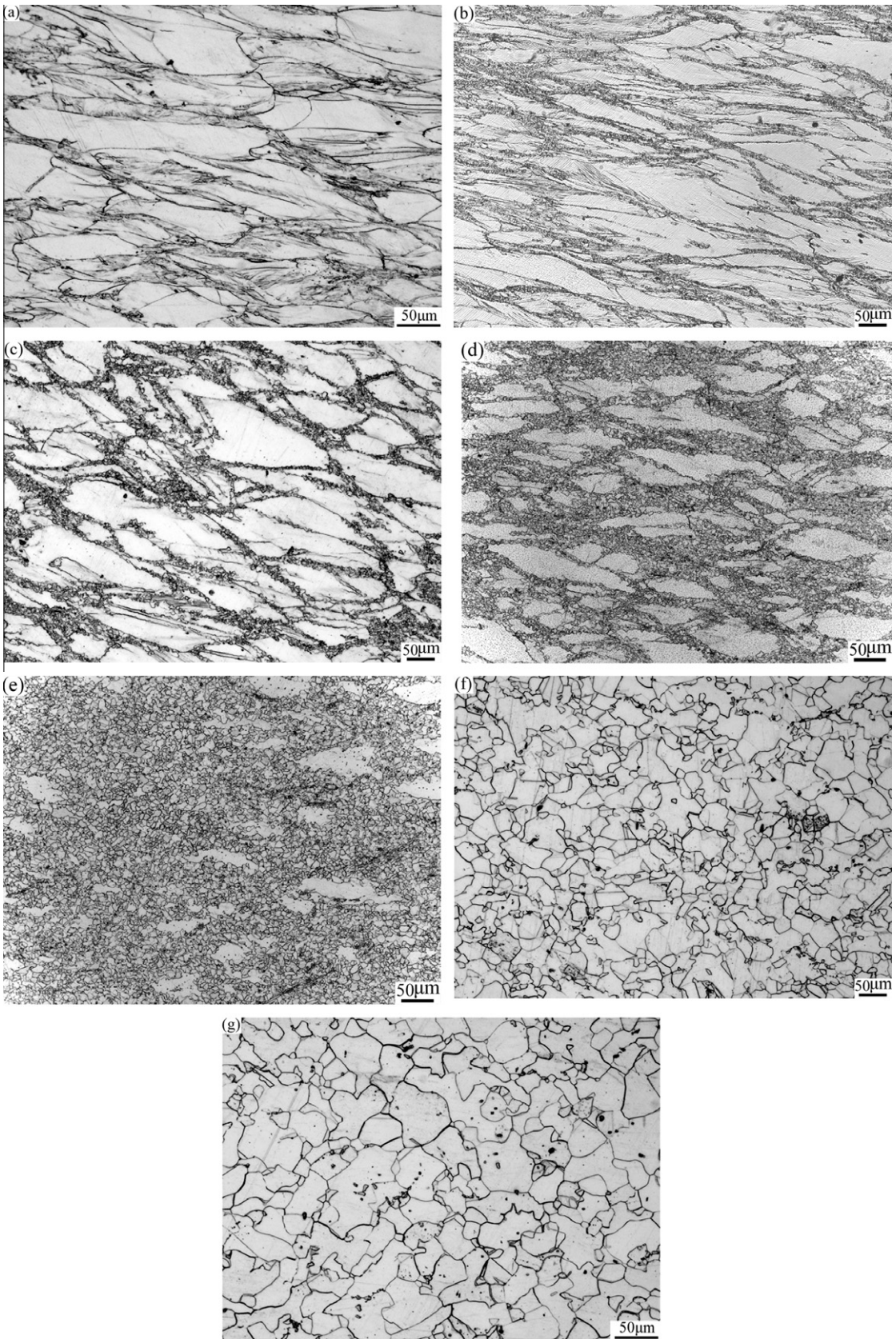

Fig. 4. Optical micrographs of Inconel 625 superalloy deformed to a 0.7 true strain at different temperatures with a strain rate of 0.1 s^{-1}: (a) 900 °C, (b) 950 °C, (c) 1000 °C, (d) 1050 °C, (e) 1100 °C, (f) 1150 °C and (g) 1200 °C.

although only a few recrystallized grains are observed at the pre-existing boundaries as well, indicating that DRX process is involved. With increasing the deformation temperature, the volume fraction of recrystallized grains increases, which are along the

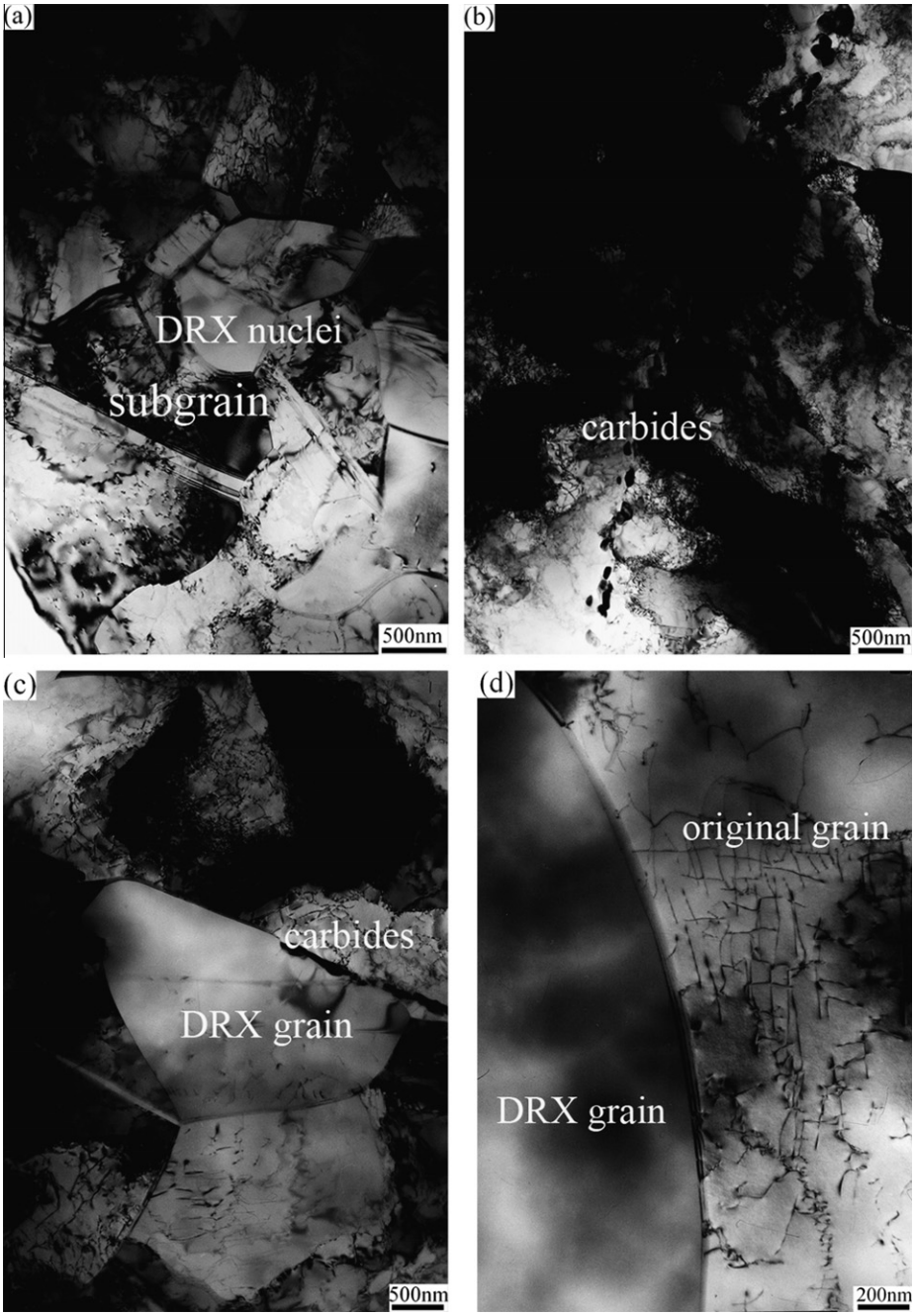

Fig. 5. TEM micrographs of Inconel 625 superalloy deformed to a 0.7 true strain at different temperatures with a strain rate of 0.1 s^{-1}: (a), (b) 1000 °C, (c) 1100 °C and (d) 1150 °C.

boundaries and form the necklace structures (as shown in Fig. 4b–e). When the deformation temperature increases to 1150 °C, the specimen has been fully recrystallized during deformation process (as shown in Fig. 4f). Thus, it is reasonable that the peak stress decreases with increasing deformation temperature, as shown in Fig. 3. Additionally, the size of recrystallized grains increases with increasing the deformation temperature, which might correlates the quickly migration of DRX grain boundaries at higher deformation temperatures.

The TEM micrographs of Inconel 625 superalloy deformed to a 0.7 true strain at different temperatures with a strain rate of 0.1 s^{-1} are shown in Fig. 5. Bulging of the original grain boundaries and subgrains in the original grains are observed. It is also found that many intergranular carbides exists along the grain boundaries at deformation temperature below 1150 °C, as shown in Fig. 5b and c. When the alloy deformed at 1150 °C, no carbides is observed (as shown in Fig. 5d). Thus, 1150 °C could be selected as the best deformation temperature, to avoid the influence of carbides on the microstructure evolution and mechanism of DRX.

3.3. The effect of deformation strain on dynamic recrystallization

Fig. 6 shows the microstructure of Inconel 625 superalloy deformed to various true strains ranging from 0.1 to 1.2 at 1150 °C at a strain rate of 0.1 s^{-1}. When the specimen was deformed to a

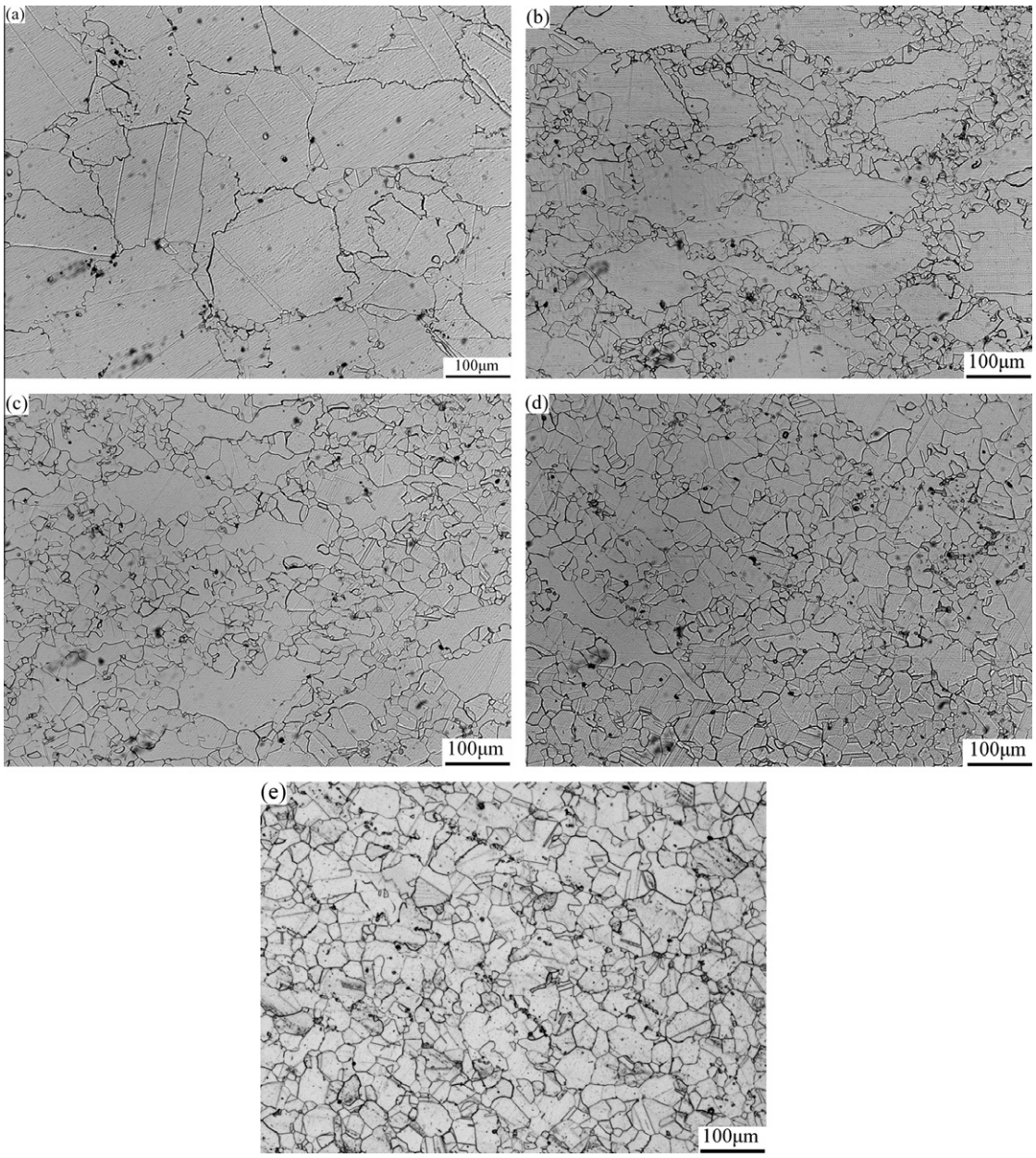

Fig. 6. Optical micrographs of Inconel 625 superalloy deformed to various strains ranging from 0.1 to 1.2 at 1150 °C with a strain rate of 0.1 s^{-1}: (a) 0.1, (b) 0.3, (c) 0.5, (d) 0.9 and (e) 1.2.

0.1 true strain, it is found that the original grain boundaries become serrated and bulging, and a few dynamically recrystallized grains are also observed along the grain boundaries (as shown in Fig. 6a). With increasing the deformation strain to 0.3, more recrystallized grains are observed along the deformed grain boundaries (as shown in Fig. 6b). As stated above and shown in Fig. 4f, the specimen has been fully recrystallized after deformation to a 0.7 true strain. Thus, the microstructure consists of both work hardened grains and dynamically recrystallized grains when the deformation strain is below 0.7. The fraction of new recrystallized grains increases gradually with increasing the deformation strains (as shown in Figs. 6a–c and 4f). However, the size of dynamically recrystallized grains remains almost constant in the range of 19–24 μm (as shown in Figs. 6a–e and 4f), which is in good agreement with previous reports based on the necklace mechanism [15,21].

3.4. Mechanisms of dynamic recrystallization

3.4.1. Bulging of the original grain boundaries

More detailed information about DRX nucleation can be obtained from the OIM maps [22–25]. Fig. 7 displays the typical OIM maps of the annealed specimen and specimens deformed to different strains ranging from 0.1 to 1.2 at 1150 °C with a strain rate of 0.1 s^{-1}. As shown in Fig. 7a, a large amount of high angle boundaries (thick black line) and only a small amount of low angle boundaries (thin grey line) are observed in the annealed superalloy. The initiation of DRX in Inconel 625 superalloy is characterized by extensively bulging grain boundaries with high angle (as shown in Fig. 7b), which is closely related to the strain induced grain boundary migration [15]. Such grain boundary morphology implies that the nucleation mechanism of DRX for Inconel 625 superalloy during hot deformation belongs to the discontinuous dynamic

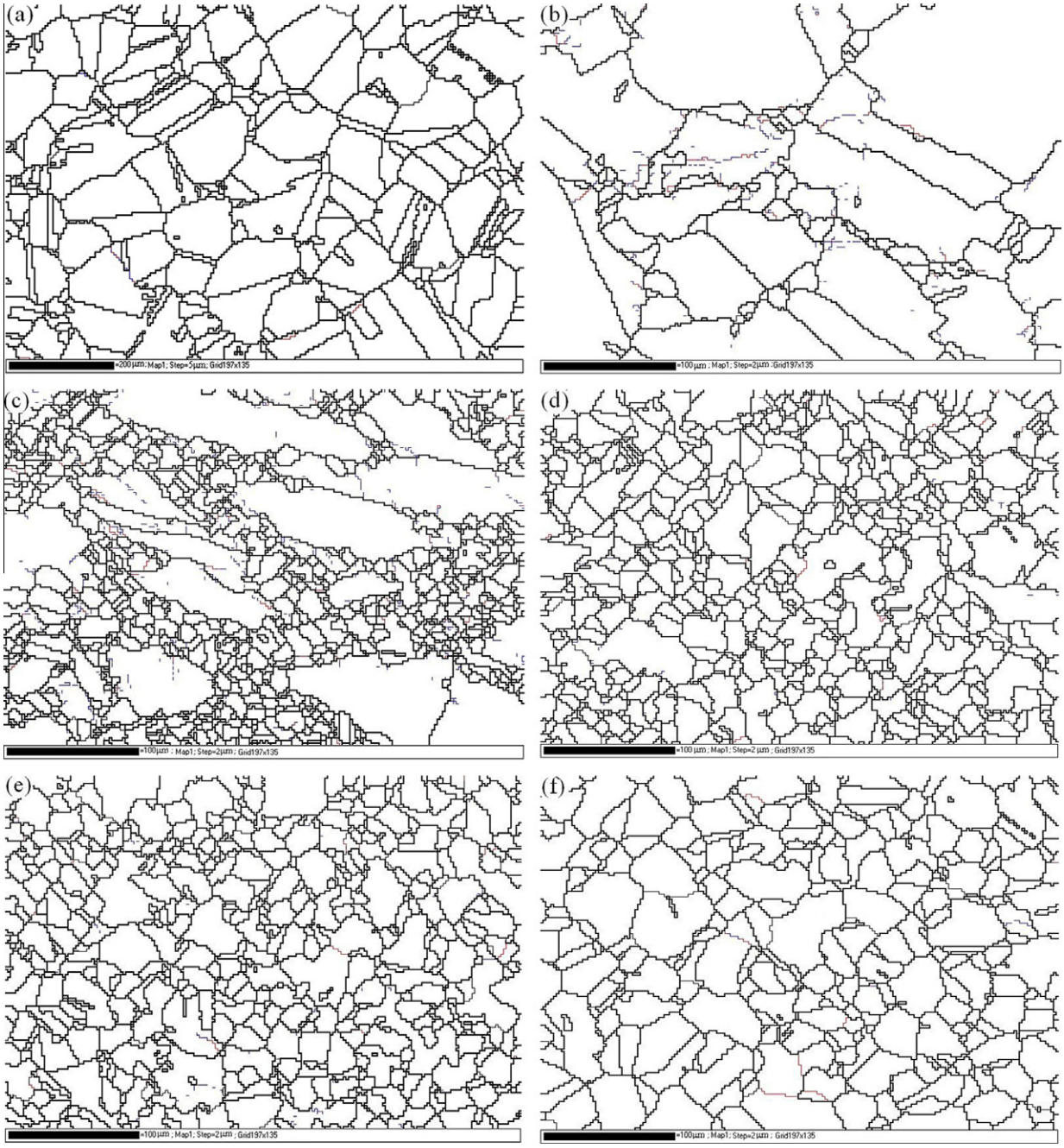

Fig. 7. Typical OIM maps of the annealed specimen and specimen deformed to different strains ranging from 0.1 to 1.2 at 1150 °C with a strain rate of 0.1 s^{-1}: (a) annealed, (b) 0.1, (c) 0.3, (d) 0.5, (e) 0.7 and (f) 1.2.

recrystallization (DDRX). However, some characteristics of the continuous dynamic recrystallization (CDRX) can also be observed in Fig. 7b, such as the subgrains with low angle boundaries frequently appear adjacent to the bulging parts of the original grain boundaries, and the individual high angle boundaries appear in the interiors of original grain. With the strain increases to 0.3, more high angle boundaries are observed along the original grain boundaries (as shown in Fig. 7c), which is consistent with the metallographic observations (as shown in Fig. 6b). The fraction of dynamically recrystallized grains increases with larger deformation strain, while there seems no change in the mount of subgrains and individual high angle boundaries in the interiors of original grain(as shown Fig. 7d–f), suggesting that DDRX is the operating mechanism of DRX.

3.4.2. Progressive subgrain rotation

The misorientation angle distributions of hot-deformed Inconel 625 superalloy are shown in Fig. 8. Compared with the annealed specimen (as shown in Fig. 8a), there is a significant increase of the misorientation at low angle boundaries which is formed during the initial stage of deformation (as shown in Fig. 8b). However, the relative frequency of the misorientation at low angle boundaries begins to decrease when the strain is larger than 0.1 ($\varepsilon > 0.1$) (as shown in Fig. 8c–f). Such a trend implies the predominant accumulation of low angle boundaries at the early stage of hot deformation and the acceleration of transformation from low angle boundaries to high angle boundaries after the peak strain. It is revealed from the misorientation angle distributions that CDRX also acts as a nucleation mechanism during hot deformation.

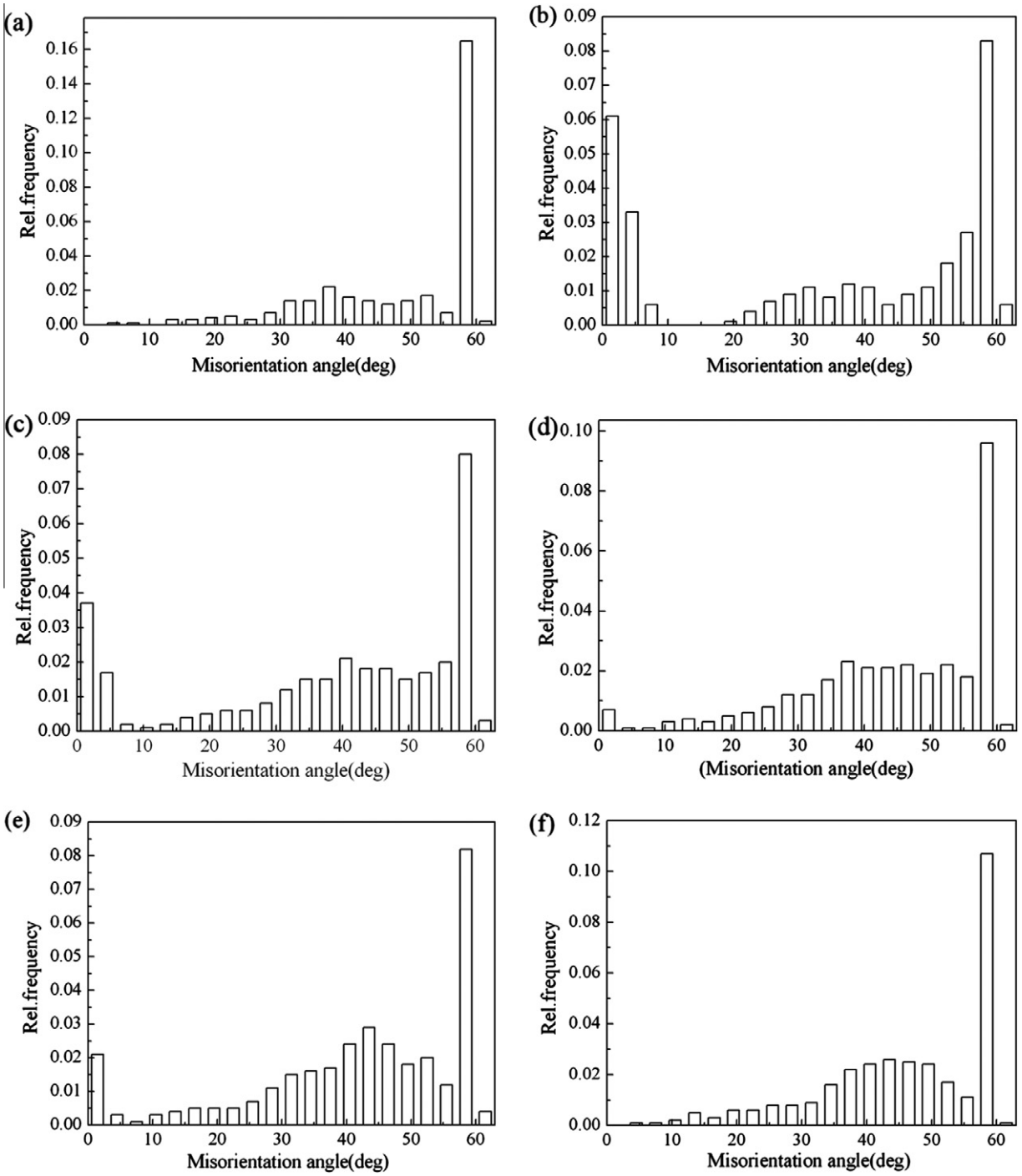

Fig. 8. Misorientation distribution histogram as a function of strain developed in Inconel 625 superalloy deformed at 1150 °C with a strain rate of 0.1 s^{-1}: (a) annealed, (b) 0.1, (c) 0.3, (d) 0.5, (e) 0.7 and (f) 1.2.

It has been pointed out that the nucleation of CDRX can be operated through progressive lattice rotation if the misorientation angles between grain boundaries are in the range from 10° to 15° [15,26]. The change of the relative frequency for different misorientation angle scope with increasing strain is summarized in Fig. 9. Nearly no subgrains with misorientation angles larger than 10° can be found with a 0.1 true strain, implying that most of the subgrain boundaries are under development. When the true strain increases from 0.1 to 0.5, the relative frequency of misorientation angle in the range of 10–15° increases from 0.01% to 2.2%, but does not change significantly with larger strain, as illustrated in Fig. 9. Therefore, a progressive subgrain rotation which will lead to the formation of nucleus in subgrain structures can only be considered as an assistant nucleation mechanism of DRX for Inconel 625 superalloy at the early stage of hot deformation.

3.4.3. Twin boundary

Figs. 6 and 7 show that newly formed twins always exist between dynamically recrystallized grains and the original ones. It has been reported that the formation of twinning plays an impor-

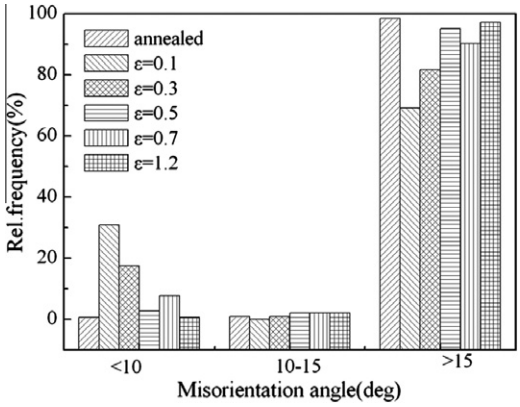

Fig. 9. Relative frequency at different mistorientation angle scopes for Inconel 625 superalloy deformed to different strains at 1150 °C with a strain rate of 0.1 s^{-1}.

tant role for the nucleation process during DRX in materials with low stacking fault energy [27,28]. Higher grain boundary mobility results in the nucleation of the twins, which acts as the main activate nucleation mechanism of DRX for nickel-based superalloy deformed at higher temperatures, accelerating the bulging and the separation of bulged parts from original grains [16]. The newly formed twins between the DRX grains and deformed grains in the annealed specimen and the hot-deformed specimen are presented in the OIM maps of Fig. 10. Comparing Fig. 10a with Fig. 10b, it is found that the amount of twin boundaries (represented in pink lines) in the initial stage of hot deformation decreases sharply than that in the annealed specimen, which is related to the loss of the twin character of original twin boundaries caused by the rotation of grains. Higher grain boundary mobility leads to the nucleation of twins generated between the original boundary and recrystallized grains. Thus, the amount of twin boundaries increases when the strain increases to 0.3 (as shown in Fig. 10c). The amount of the twin boundaries decreases again with the strain increasing to 0.7 (as shown in Fig. 10d), indicating that the progressive transformation of twin boundaries into random high angle boundaries owing to an interaction between mobile dislocations and twin boundaries. This phenomenon also implies that the formation of twins can active the nucleation of DRX for Inconel 625 superalloy at the early stage of hot deformation.

3.5. Confirmation of nucleation mechanisms

The grain structures and the dislocation substructures of Inconel 625 superalloy deformed to different strains at higher temperature were examined by TEM to further confirm the nucleation mechanisms of DRX. TEM micrographs of specimens compressed to various strains under the DRX condition are presented in Fig. 11, from which the serrated grain boundaries, fine subgrains and twins can be clearly observed.

The tangled dislocation walls are found along the original grain boundaries with the strain of 0.1, leading to the formation of bulging out part of the serrated grain boundaries, as shown in Fig. 11a. The recrystallized grains were formed at these locations, implying that DDRX takes place in hot-deformed Inconel 625 superalloy. Meanwhile, the subgrains and twins are also observed in the original grains (as shown in Fig. 11b and c), suggesting that the nucleation mechanisms of subgrain rotation and formation of twining also occur at the initial stage of deformation. With further deformation, dislocations formed inside the original grains can easily move to the places near the original grain boundaries due to the

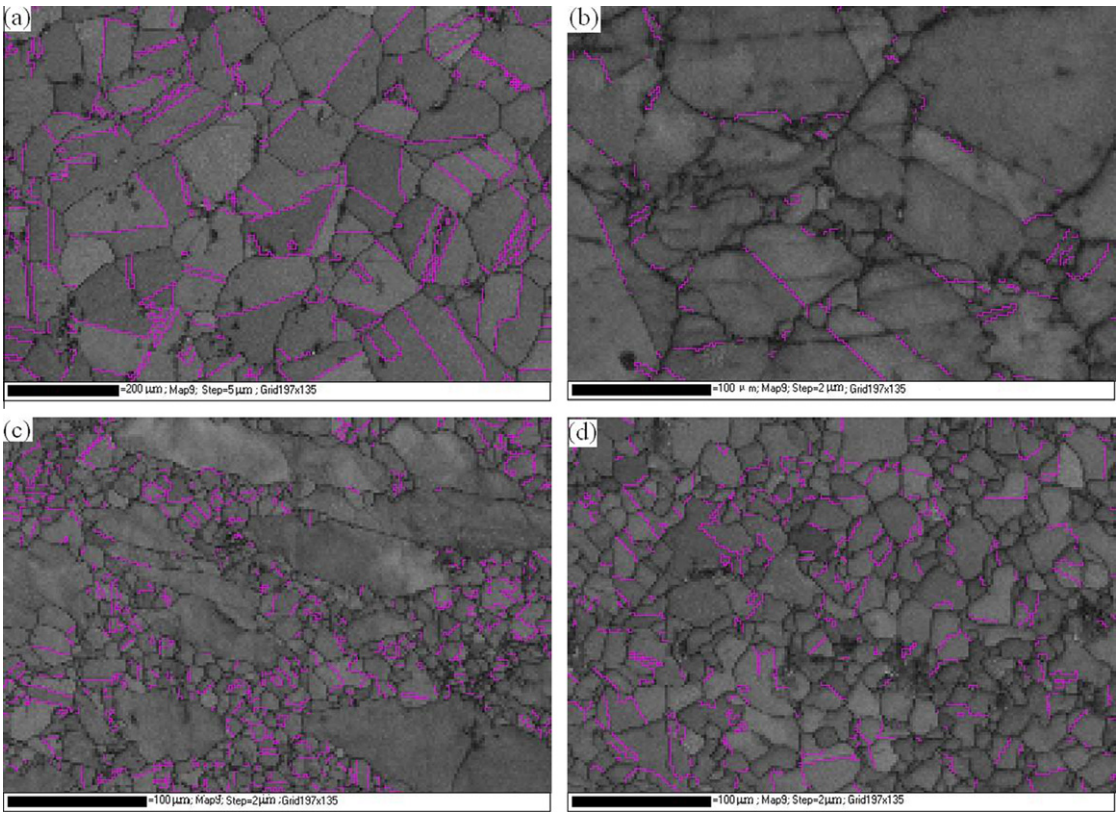

Fig. 10. OIM maps show the twin boundaries of the annealed specimen and specimen deformed to different strains at 1150 °C at a strain rate of 0.1 s^{-1}: (a) annealed, (b) 0.1, (c) 0.3 and (d) 0.7.

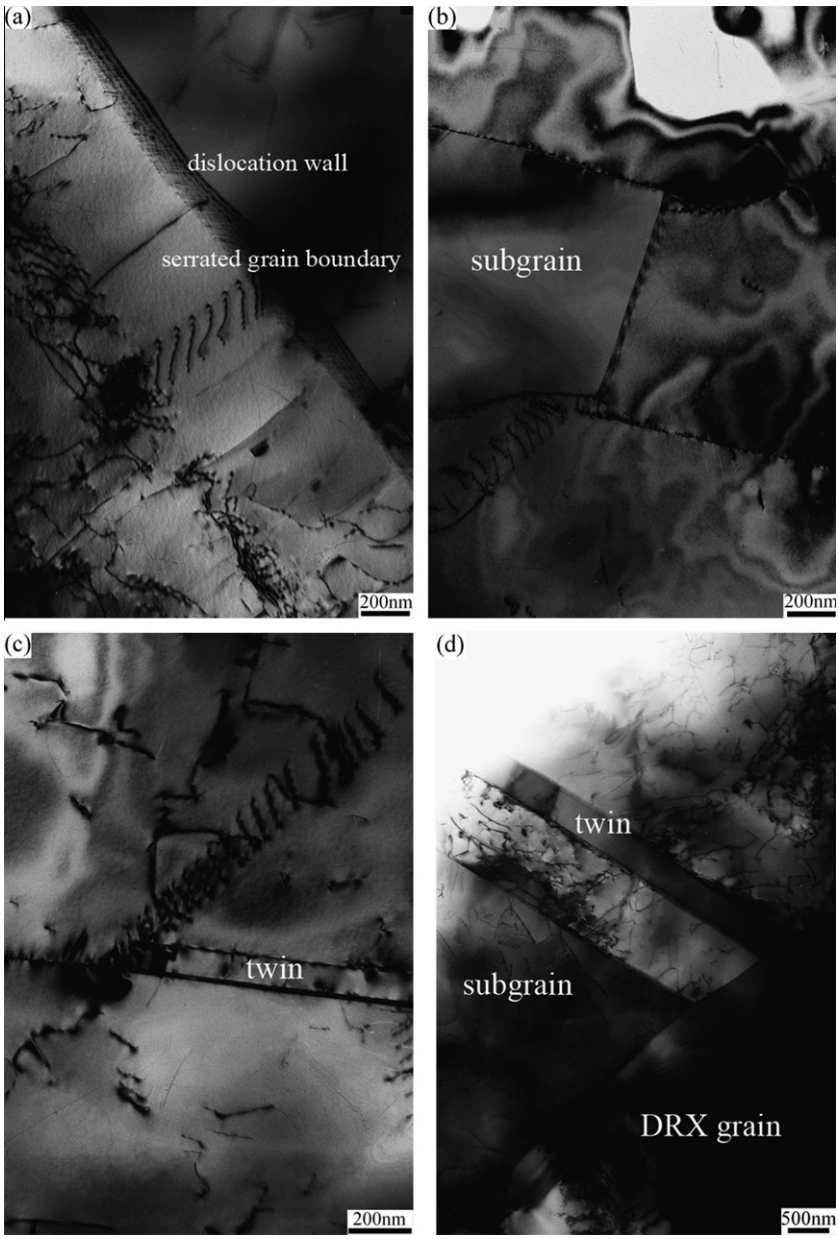

Fig. 11. TEM micrographs of Inconel 625 superalloy deformed to different strains at 1150 °C with a strain rate of 0.1 s^{-1}. (a), (b) and (c) 0.1 and (d) 0.5.

low stacking fault energy of this alloy, resulting in the simultaneous occurrence of the CDRX and DDRX in the vicinity of the original grain boundary (as shown in Fig. 11d).

4. Conclusions

(1) The size and fraction of the DRX grains in hot-deformed Inconel 625 superalloy increases with increasing the deformation temperature. No carbides is observed when the deformation temperature increasing to 1150 °C.

(2) The original deformed grains have completely turned into equiaxed DRX grains when the specimen deformed to a 0.7 true strain at 1150 °C with a strain rate of 0.1 s^{-1}. The fraction of the DRX grains in Inconel 625 superalloy increases with increasing the deformation strain before the grains are fully recrystallized. However, the size of DRX grains almost remains constant, in the range of 19–24 μm, irrespective of the deformation strain.

(3) DDRX characterized by bulging of the original grain boundaries accompanied with twining is the dominant nucleation mechanism of DRX for Inconel 625 superalloy deformed at 1150 °C. CDRX with subgrain rotation in the vicinity of the serrated grain boundaries occurs simultaneously with DDRX, which can only be considered as an assistant nucleation mechanism of DRX at the early stage of hot deformation.

References

[1] Mittra J, Dubey JS, Banerjee S. Acoustic emission technique used for detecting early stages of precipitation during aging of Inconel 625. Scripta Mater 2003;49:1209–14.
[2] Shankar V, Bhanu Sankara Rao K, Mannan SL. Microstructure and mechanical properties of Inconel 625 superalloy. J Nucl Mater 2001;288:222–32.
[3] Dinda GP, Dasgupta AK, Mazumder J. Laser aided direct metal deposition of Inconel 625 superalloy: microstructural evolution and thermal stability. Mater Sci Eng A 2009;509:98–104.

[4] Cai DY, Xiong LY, Liu WC, Sun GD, Yao M. Characterization of hot deformation behavior of a Ni-base superalloy using processing map. Mater Des 2009;30:921–5.
[5] Tian GF, Jia CC, Liu JT, Hu BF. Experimental and simulation on the grain growth of P/M nickel-base superalloy during the heat treatment process. Mater Des 2009;30:433–9.
[6] Zhu ML, Xuan FZ, Wang GZ. Effect of microstructure on fatigue crack propagation behavior in a steam turbine rotor steel. Mater Sci Eng A 2009;515:85–92.
[7] Kwong J, Axinte DA, Withers PJ. The sensitivity of Ni-based superalloy to hole making operations: influence of process parameters on subsurface damage and residual stress. J Mater Process Technol 2009;209:3968–77.
[8] Medeiros SC, Prasad YVRK, Frazier WG, Srinivasan R. Microstructural modeling of metadynamic recrystallization in hot working of IN 718 superalloy. Mater Sci Eng A 2000;293:198–207.
[9] Zhang Y, Zeng XQ, Lu C, Ding WJ. Deformation behavior and dynamic recrystallization of a Mg–Zn–Y–Zr alloy. Mater Sci Eng A 2006;428:91–7.
[10] Fatemi-Varzaneh SM, Zarei-Hanzaki A, Beladi H. Dynamic recrystallization in AZ31 magnesium alloy. Mater Sci Eng A 2007;456:52–7.
[11] Sitdikov O, Kaibyshev R. Dislocation glide and dynamic recrystallization in LiF single crystals. Mater Sci Eng A 2002;328:147–55.
[12] McQueen HJ. Development of dynamic recrystallization theory. Mater Sci Eng A 2004;387–389:203–8.
[13] Sakai T, Miura H, Goloborodko A, Sitdikov O. Continuous dynamic recrystallization during the transient severe deformation of aluminum alloy 7475. Acta Mater 2009;57:153–62.
[14] Belyakov A, Tsuzaki K, Miura H, Sakai T. Effect of initial microstructures on grain refinement in a stainless steel by large strain deformation. Acta Mater 2003;51:847–61.
[15] Humphreys FJ, Hatherly M. Recrystallization and related annealing phenomena. Oxford: Pregamon Press; 2004.
[16] Wang Y, Shao WZ, Zhen L, Zhang XM. Microstructure evolution during dynamic recrystallization of hot deformed superalloy 718. Mater Sci Eng A 2008;486:321–32.
[17] Wang Y, Shao WZ, Zhen L, Yang L, Zhang XM. Flow behavior and microstructures of superalloy 718 during high temperature deformation. Mater Sci Eng A 2008;497:479–86.
[18] Doherty RD, Hughes DA, Humphreys FJ, Jonas JJ, Juul Jensen D, Kassner ME, et al. Current issues in recrystallization: a review. Mater Sci Eng A 1997;238:219–74.
[19] Sakai T. Dynamic recrystallization microstructures under hot working conditions. J Mater Process Technol 1995;53:349–61.
[20] Poliakt EI, Jonass JJ. A one-parameter approach to determining the critical conditions for the initiation of dynamic recrystallization. Acta Mater 1996;44(1):127–36.
[21] Kim SI, Yoo YC. Dynamic recrystallization behavior of AISI 304 stainless steel. Mater Sci Eng A 2001;311:108–13.
[22] Yamagata H, Ohuchida Y, Saito N, Otsuka M. Nucleation of new grain during discontinuous dynamic recrystallization of 99.998 mass% aluminum at 453 K. Scripta Mater 2001;45:1055–61.
[23] Du YX, Zhang XM, Ye LY, Luo ZH. Recrystallization behavior of high purity aluminum at 300 °C. Trans Nonferrous Metall Soc Chin 2006;16:1307–12.
[24] Yang P. Electron backscattered diffraction technology and application. Beijing: Metallurgy Industry Press; 2007.
[25] Kaibyshev R, Shipilova K, Musin F, Motohashi Y. Continuous dynamic recrystallization in an Al–Li–Mg–Sc alloy during equal-channel angular extrusion. Mater Sci Eng A 2005;396:341–51.
[26] Ponge D, Gottstein G. Necklace formation during dynamic recrystallization: mechanisms and impact on flow behavior. Acta Metall 1998;46:69–80.
[27] Gottstein G, Kocks UF. Dynamic recrystallization and dynamic recovery in ⟨1 1 1⟩ single crystals of nickel and copper. 1983; 31. p. 175–88.
[28] Sample VM, Fitzsimons GL, DeArdo AJ. Dynamic softening of copper during deformation at high temperatures and strain rates. Acta Metall 1987;35: 367–79.